IOPscience iopscience.iop.org

Home Search Collections Journals About Contact us My IOPscience

Unipolar Resistive Switching in ZrO_2 Thin Films

This content has been downloaded from IOPscience. Please scroll down to see the full text.

2013 Jpn. J. Appl. Phys. 52 041101

(http://iopscience.iop.org/1347-4065/52/4R/041101)

View the table of contents for this issue, or go to the journal homepage for more

Download details:

IP Address: 140.113.38.11
This content was downloaded on 26/04/2014 at 06:58

Please note that terms and conditions apply.

Japanese Journal of Applied Physics **52** (2013) 041101 **REGULAR PAPER**
http://dx.doi.org/**10.7567/JJAP.52.041101**

Unipolar Resistive Switching in ZrO_2 Thin Films

Guo-Yong Zhang[1], Dai-Ying Lee[1], I-Chuan Yao[2], Chung-Jung Hung[2], Sheng-Yu Wang[1], Tai-Yuen Huang[1], Jia-Woei Wu[1], and Tseung-Yuen Tseng[1*]

[1] *Department of Electronics Engineering and Institute of Electronics, National Chiao Tung University, Hsinchu 300, Taiwan*
[2] *Department of Materials Science and Engineering, National Chiao Tung University, Hsinchu 300, Taiwan*
E-mail: tseng@cc.nctu.edu.tw

Received November 26, 2012; accepted January 21, 2013; published online March 14, 2013

Unipolar resistive switching behaviors including bistable memory switching and monostable threshold switching were found in ZrO_2 thin films fabricated by a simple sol–gel method with the $Ti/ZrO_2/Pt$ structure. The multilevel resistive switching behaviors were also revealed by varying the compliance current from 9 to 38 mA. Physical mechanisms based on a conductive filament model were proposed to explain the resistive switching phenomena and the device breakdown. A figure of merit $Z = \rho_a/\rho_f$ was defined as a criterion for evaluating OFF/ON resistance ratio, where ρ_f and ρ_a represent the resistivities of the conductive filament and the fracture region of the filament, respectively. The advantages such as unipolar resistive switching, multilevel resistive switching, good scalability, low operation voltage (<5 V), high OFF/ON resistance ratio (> 10^3), nondestructive readout, long retention (> 10^4 s), and simple fabrication method make the ZrO_2-based resistive switching device a promising candidate for next-generation nonvolatile memory applications. © 2013 The Japan Society of Applied Physics

1. Introduction

Nonvolatile memories (NVMs) have become a key part of modern information technology devices since they were invented by Kahng and Sze at Bell Labs in 1967.[1,2] Nowadays, they are widely used in portable devices such as cell phones, digital cameras, tablet personal computers, and notebook computers. However, conventional NVMs such as the charge-storage-based FLASH memories will meet their physical limitations as the devices are scaling down.[3–5] To overcome this bottleneck, several emerging memories including magnetic random access memory (MRAM), ferroelectric random access memory (FRAM), phase-change random access memory (PRAM), and resistive random access memory (RRAM), have been proposed as candidates for next-generation memories.[6,7] Among these novel devices, the RRAM that is composed of a simple metal–insulator–metal (M–I–M) capacitor structure has been intensively studied because of its merits of low power consumption, low-voltage and high-speed operation, high endurance, long retention, high packing density, nondestructive readout, and low cost.[3–5]

Resistive switching is a universal phenomenon arising in conductor/nonconductor/conductor system upon application of proper electrical voltage or current signals.[6,8–10] Resistive switching can be either bistable memory switching or monostable threshold switching.[11,12] On the basis of polarity, it can be classified into three modes: unipolar, bipolar, and nonpolar switching.[7,13–15] Unipolar (or nonpolar) memory switching has special importance because it can be used to design high-density cross-bar RRAM devices by employing the one diode and one resistor (1D1R) architecture, which is believed to be a promising memory concept.[16,17] Nonconducting materials including both organic and inorganic materials have demonstrated good switching properties,[6] such as organic materials (small organic semiconducting molecules, polymers and composites containing nanoparticles),[18] perovskite oxides ($La_{0.7}Ca_{0.3}MnO_3$,[19] $Sm_{0.7}Ca_{0.3}MnO_3$,[20] and $Pr_{0.7}Ca_{0.3}MnO_3$[21]) and binary oxides (ZrO_2,[15,22–32] CeO_2,[33] Cu_xO,[34] Ga_2O_3,[35] Eu_xO_y,[36] NiO,[11,37] TaO_x,[38] Al_2O_3,[39,40] Al_xO_y,[41] MnO_2,[42] HfO_2,[43–45] TiO_2,[46,47] ZnO,[48] and Nb_2O_5[49]). Among these materials, binary oxides have great advantages because they have the superior merits of simple component, require low-temperature process, have thermal robustness, and are fully compatible with complementary metal oxide semiconductor (CMOS) technology.[24,50] Therefore, the unipolar resistive switching in binary oxides is more attractive and valuable for developing high-performance RRAM devices.

Research on RRAM mainly focuses on six aspects: 1) switching mechanisms, 2) switching materials, 3) switching characteristics, 4) electrodes, 5) device structures, and 6) fabrication methods. Up to now, magnetron sputtering,[3–5,13,15,22–38,50–55] pulsed laser deposition (PLD),[19–21,43,49] plasma oxidation,[41] atomic layer deposition (ALD),[44] metallorganic chemical vapor deposition (MOCVD),[45] thermal oxidation,[47] laser molecular beam epitaxy (laser MBE),[56] physical vapor deposition (PVD),[57] and sol–gel[58,59] methods have been used to fabricate switching materials in RRAM devices. Among these techniques the sol–gel method has some advantages: simple fabrication, low cost, and low-temperature process. Recently, both unipolar and bipolar switching behaviors have been observed and studied in ZrO_2-thin-film-based RRAM devices. However, the ZrO_2 thin films were mostly deposited by a radio-frequency (RF) magnetron sputtering. In this work, the unipolar resistive switching of a Ti/sol–gel ZrO_2/Pt structure was investigated for RRAM applications. A conductive filament (CF) model was proposed to explain the switching mechanism. The multilevel resistive switching behaviors were observed by varying compliance current. The CFs had two different behaviors in the low- and high-compliance-current ranges, respectively. Furthermore, the formation of a CF network was proposed to explain the breakdown mechanism.

2. Experimental Procedure

80-nm-thick ZrO_2 thin films were deposited on $Pt/Ti/SiO_2/Si$ substrates by a simple poly(vinyl alcohol) (PVA) sol–gel route. The starting materials were zirconium acetate [$Zr(CH_3COO)_4$] in dilute acetic acid (Aldrich 413801), PVA (average molecular weight, 2000), and distilled water. PVA is used because it is an environmentally friendly material. The typical procedure is shown in Fig. 1. For electrical

 © 2013 The Japan Society of Applied Physics

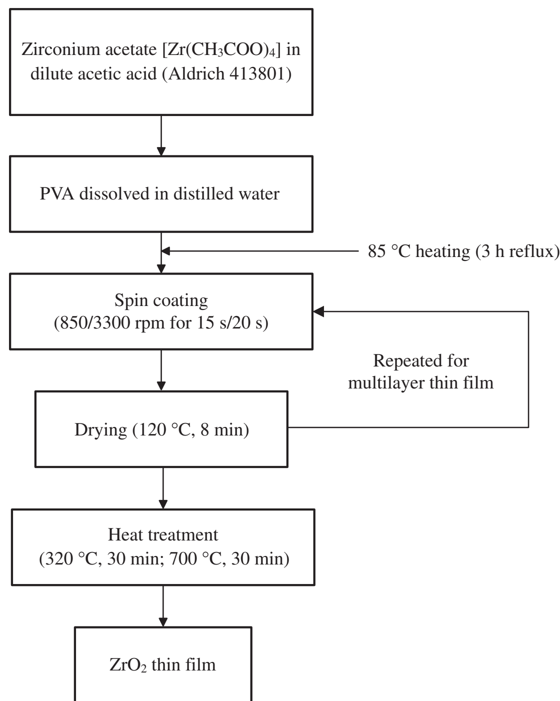

Fig. 1. Sol–gel route for preparation of ZrO_2 thin films.

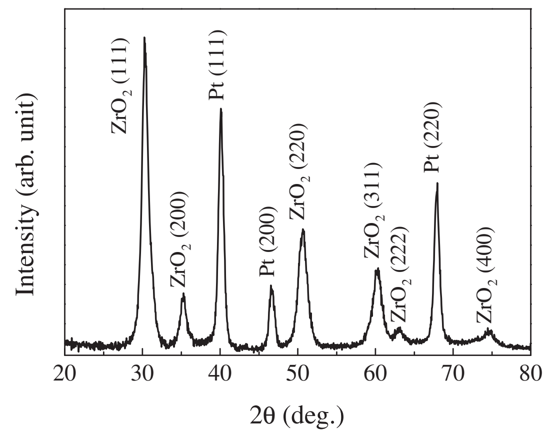

Fig. 2. XRD spectra of a ZrO_2 film on Pt.

measurements, disk-shaped Ti electrodes were fabricated on the top of the ZrO_2 thin films using e-gun at the same thickness of 100 nm and three different diameters (150, 250, and 350 μm). Unless otherwise specifically stated, all the top electrodes of the devices used in the experiments have a diameter of 350 μm. Current–voltage (I–V) curves were measured using an Agilent 4155C semiconductor parameter analyzer at room temperature. The Ti top electrode was grounded and a positive bias voltage V_s was applied on the Pt bottom electrode.

3. Results and Discussion

X-ray diffraction patterns show that the ZrO_2 thin film has a polycrystalline structure (Fig. 2). The as-deposited ZrO_2 thin film is an insulator; however, during the forming process, when a forming voltage, V_{form} of 10.5 V was applied, there was a sudden increase in current [Fig. 3(a)], indicating that a conducting path was created in it. During the forming process, a compliance current (I_{comp}) of 3 mA was applied to prevent the device from breaking down. After the forming process, the device was switched from the high-resistance state (HRS or "OFF" state) to the low-resistance state (LRS or "ON" state), which can also be called the first SET process. Thereafter, as V_s swept again in the same positive direction, the RESET process happened at 2.8 V (RESET voltage, V_{reset}) with $I_{reset} = 40$ mA (RESET current) where the ON state was switched to the OFF state. During the subsequent cycles, the switching between the OFF and ON states occurred alternatively by applying V_{set} (SET voltage) and V_{reset}. It should be noted that only the SET process needs compliance current. In the RESET process, compliance current is never applied. Because both the OFF and ON states can be maintained without any bias, they are both nonvolatile memory states. During the switching processes the bias direction keeps unchanged; therefore, the switching is unipolar. The ratio $r = R_{off}/R_{on}$ is as high as 2.19×10^3 at 0.3 V read voltage (V_{read}), where R_{off} and R_{on} are the OFF and ON state resistances, respectively. The inset in Fig. 3(a) shows the top electrode area dependence of R_{off}, R_{on}, and r. R_{off} decreases as the area increases, while R_{on} is nearly independent of the area, indicating that the conducting path is localized rather than uniform, which can be called CF. Owing to the CF mechanism, r increases with decreasing area. In fact, under a high electrical field applied to ZrO_2 thin films, the oxygen ions will migrate towards the bottom electrode[13] and oxygen vacancies will connect to each other to form the CF, which is the micromechanism of the forming (SET) process [Fig. 3(b)]. For the RESET process, it is the Joule heating that provides the energy for oxygen ions to recombine with oxygen vacancies, as a result the CF ruptures [Fig. 3(b)]. Here, although the CF usually has an irregular shape, we study the CF assuming a line shape for simplicity. Besides such size-dependent properties, other switching properties of RRAM can also be enhanced as the area decreases, such as increased stability and decreased working current and variation, which make the Mole law still effective; however, for conventional memory devices such as DRAM and FLASH, the Mole law will not work because they are approaching their physical limitations.[60)]

Figure 4 shows typical stress test results. During the stress test, a small 10 mV V_{read} was applied every 10 s for a total of 1.08×10^4 s. It can be seen from the figure that both R_{off} and R_{on} are stable, and between them a clear ratio window exists. Initially, as t increases, R_{off} increases steadily owing to a slow recombination of oxygen ions and oxygen vacancies. At 10,340 s, there is a sudden increase in R_{off}, indicating the occurrence of an obvious recombination; although thereafter R_{off} decreases owing to the migration of oxygen vacancies, it remains high, which ensures the high OFF/ON resistance ratio. For R_{on} on the other hand, at the beginning it is stable, but immediately after, it shows a small but sudden increase at 140 s owing to an obvious recombination, and then it remains nearly unvaried, showing a high stability. Taken together, although there are some variations, both R_{off} and R_{on} maintain a clear ratio window ($r_w = 24\times$) for more than 10^4 s, which demonstrated that their nondestructive readout properties are stable against read operation.

Another interesting phenomenon is that in some samples a monostable threshold switching can be observed besides the

© 2013 The Japan Society of Applied Physics

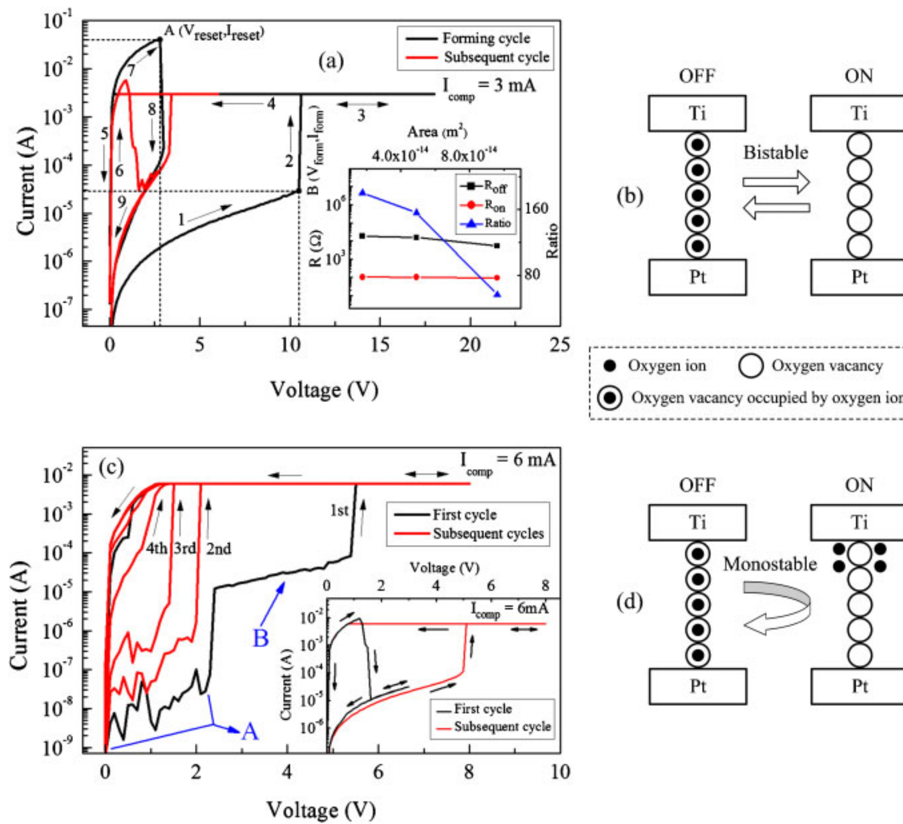

Fig. 3. (Color online) (a) Bistable memory switching. The inset shows the Ti top electrode area dependence of R_{off}, R_{on}, and OFF/ON resistance ratio. (b) CF model for bistable memory switching. (c) Monostable threshold switching. The inset shows the bistable memory switching. The bistable memory switching was turned into the monostable threshold switching in a stress test. (d) CF model for monostable threshold switching. In the ON state near the CF, the oxygen ion concentration is higher than that in bistable memory switching.

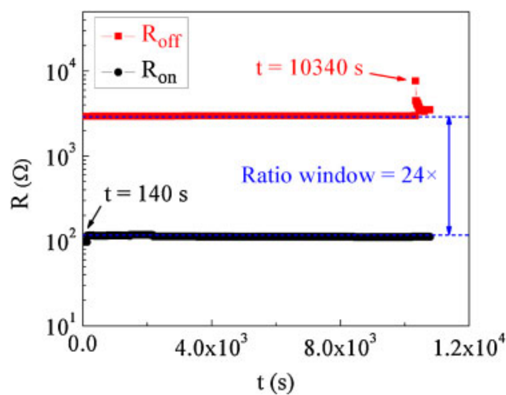

Fig. 4. (Color online) Typical stress test results for R_{off} and R_{on} with $V_{read} = 10$ mV. R_{off} (R_{on}) suddenly increases at $t = 10340$ (140) s.

bistable unipolar memory switching [Fig. 3(c)]. Firstly, a reproducible bistable memory switching was measured [inset in Fig. 3(c)]. Secondly, the ON state was subjected to a stress test at a low 50 mV V_{read} applied every 10 s for a total of 1.08×10^4 s. Thereafter, it was found that the device only shows a monostable threshold switching in the first four cycles (labeled as 1st–4th). In the 1st cycle the device was switched ON with $I_{comp} = 6$ mA; however, the ON state could not be maintained when the power was turned off and the 2nd cycle started in the OFF state. It was the same for the 3rd and 4th cycles. This is the monostable threshold switching: the ON state is not stable and always switches to the OFF state when the power is turned off. It is suggested that oxygen vacancy concentration could play a key role in determining the switching behaviors. If the concentration is high, the CF will be thick and the ON state will be stable; however, the RESET process will consume more electrical energy. On the other hand, at a low concentration, the CF will become weak and can rupture easily; therefore, bistable switching can become monostable switching or even non-switching. We assume that in such a sample there is a relatively low oxygen vacancy concentration, and at a low V_{read} the recombination between oxygen ions and oxygen vacancies occurs and the CF ruptures. Since the fracture region is very thin, even a low V_{read} can generate a relatively high electrical field to drive the oxygen ions to migrate from the Ti top electrode towards the thin fracture region and accumulate; eventually, a fracture region with a high oxygen ion concentration forms [Fig. 3(d)]. Afterwards, as the electrical field increases, in the fracture region there is a competition between the separation and recombination of oxygen ions and oxygen vacancies, which leads to some fluctuations in the "A" part of the 1st cycle. As the electrical field is reasonably high, the recombination is dominant and a flat level ("B" part) appears; as the electrical field is higher then, because now the oxygen ion concentration in the sink (interface layer) is low, oxygen ion migration becomes slow, and soft breakdown occurs in the fracture region, and the ON state is achieved finally. That is, oxygen ion concentration decreases to some degree during each switching cycle owing to the migration of oxygen ions, which decreases V_{set} as

© 2013 The Japan Society of Applied Physics

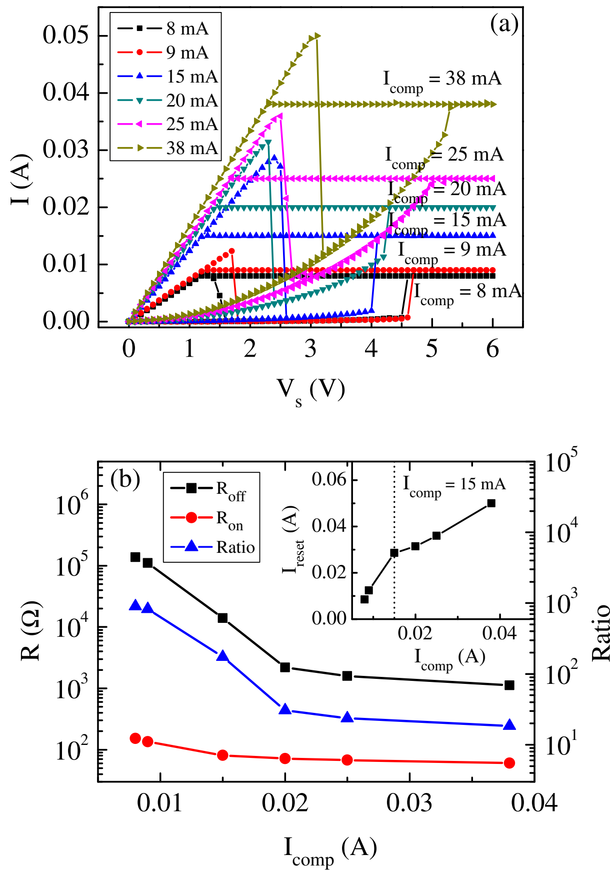

Fig. 5. (Color online) (a) I–V curves under various current compliances during SET process. (b) Compliance current dependence of R_{off}, R_{on}, and OFF/ON resistance ratio. The inset shows that I_{reset} increases with I_{comp}.

the number of switching cycles increases; therefore, the monostable threshold switching behavior is maintained.

The influence of I_{comp} on the switching properties was investigated by measuring I–V curves. Figure 5(a) shows that as I_{comp} increases the Ti/ZrO_2/Pt device demonstrates multilevel resistive switching behaviors. The multilevel resistive switching works well in a broad range of compliance currents from 8 to 38 mA, indicating that the device has a high stability against high currents. The device breaks down above 38 mA. Figure 5(b) shows that both R_{on} and R_{off} decrease as I_{comp} increases. However, R_{off} decreases much faster than R_{on}: R_{off} decreases more than two orders of magnitude (from 1.38×10^5 to 1.12×10^3 Ω), while R_{on} only decreases from 153 to 60 Ω. As a result, r decreases as I_{comp} increases. R_{on}, R_{off}, and r all demonstrate multilevel properties. The CF model can be used to explain the phenomena caused by I_{comp}. Figure 6 shows the equivalent resistances of R_{off} and R_{on}. R_f is the resistance of the CF, and R_r is the resistance of the remaining part except the CF in the ZrO_2 thin film. If we ignore R_r and only consider the CF, we obtain $r = (R_a + R_b)/R_f = (\rho_a l_a/S + \rho_f l_b/S)/(\rho_f l/S) = (\rho_a l_a)/(\rho_f l) + l_b/l$, where $\rho_a(l_a)$, ρ_f, l_b, l, and S are the resistivity (length) of the fracture region of the CF, the resistivity of the CF, the length of the residual CF, and the length and cross-sectional area of the CF, respectively. Using $l = l_a + l_b$ and $0 \le l_b < l$, we obtain $0 \le l_b/l < 1$. The fracture region is located immediately under the Ti top electrode. Because the concentration of oxygen vacancies

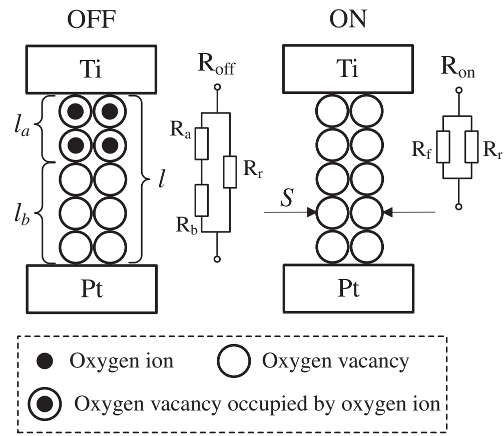

Fig. 6. Equivalent resistances of R_{off} and R_{on}.

in the Ti/ZrO_2 interface layer and the top layer of the ZrO_2 thin film is high, the oxidation can occur easily. Note that usually r is much higher than 1; therefore, by ignoring l_b/l we obtain

$$r = \frac{\rho_a l_a}{\rho_f l}. \tag{1}$$

As I_{comp} increases, the diameter of the CF increases; therefore, both R_{off} and R_{on} will decrease. However, from Eq. (1) it can be seen that r is independent of S. Furthermore, since $0 < l_a/l \le 1$, r is mainly attributed to ρ_a/ρ_f. Considering the important status of ρ_a/ρ_f, we define a new parameter, $Z = \rho_a/\rho_f$, as the figure of merit for evaluating r, and Eq. (1) can be written as $r = Zl_a/l$. $Z > r$, Z can be estimated by measuring r. For the ZrO_2-based switching device, Z is higher than 10^3. Table I shows a summary of Z-values of different switching materials. As I_{comp} increases further, more oxygen vacancies will exist in the fracture region; thus ρ_a will decrease. On the other hand, the thicker CF is not easily broken; therefore, the residual CF will become longer in the OFF state, i.e., l_a will decrease. During the switching processes, both ρ_f and l are constants; therefore, decreasing ρ_a and/or l_a can decrease r. Furthermore, as I_{comp} increases, R_r will decrease because more oxygen vacancies will be created in the thin film by the high-Joule heating, which can be another important factor that increases the conductivity of the device. Figure 7 shows the relationship between R_{off} and R_{on} at various I_{comp} values, i.e., the figure shows a phase diagram of R_{off}, R_{on}, and I_{comp}. It can be seen that R_{off} decreases monotonically with R_{on}, which can be divided into three regions on the basis of $I_{comp} = 15$ and 38 mA (note that as I_{comp} increases, R_{on} decreases): linear region ($I_{comp} < 15$ mA), nonlinear region ($15 \le I_{comp} \le 38$ mA), and breakdown region ($I_{comp} > 38$ mA). The relationship between the OFF and ON state electrical conductances (G_{off} and G_{on}) demonstrates the linear and nonlinear regions more clearly, as shown in the inset of Fig. 7. Furthermore, the inset of Fig. 5(b) shows that the I_{reset}–I_{comp} relationship is also divided into two regions on the basis of $I_{comp} = 15$ mA. These findings reflect the key role of I_{comp} in switching characteristics. The above discussion is mainly limited to the CF, and now we consider the whole thin film. When I_{comp} is small (<15 mA), there are few CFs (or only one single CF). Because the number of

 © 2013 The Japan Society of Applied Physics

Table I. Summary of Z-values of different resistive switching devices.

Switching material	Device structure	Fabrication method	Switching behavior	$Z = \rho_a/\rho_f$	Reference
ZrO_2	$Ti/ZrO_2/Pt$	Sol–gel	Unipolar	$>10^3$	This work
Nb_2O_5	Pt/Nb_2O_5/p-Si	PLD	Unipolar	$>10^2$	49
Al_xO_y	$Al/Al_xO_y/Al$	Plasma oxidation	Unipolar	$>10^4$	41
NiO	Pt/NiO/Pt	Reactive DC magnetron sputtering	Unipolar	$>10^4$	37
CeO_2	$Pt/CeO_2/Pt$	RF magnetron sputtering	Unipolar	$>10^5$	33
Eu_xO_y	$Pt/Eu_xO_y/Pt$	RF magnetron sputtering	Unipolar	$>10^8$	36
HfO_2	$Au/HfO_2/Pt$	MOCVD	Unipolar	$>10^9$	45
TiO_2	$Ag/TiO_2/Pt$	Thermal oxidation	Bipolar	$>10^8$	47
Cu–C	Pt/Cu–C/Pt	RF magnetron sputtering	Bipolar	$>10^2$	55
Cu:TCNQ	Al/Cu:TCNQ/Cu	PVD	Bipolar	$>10^3$	57

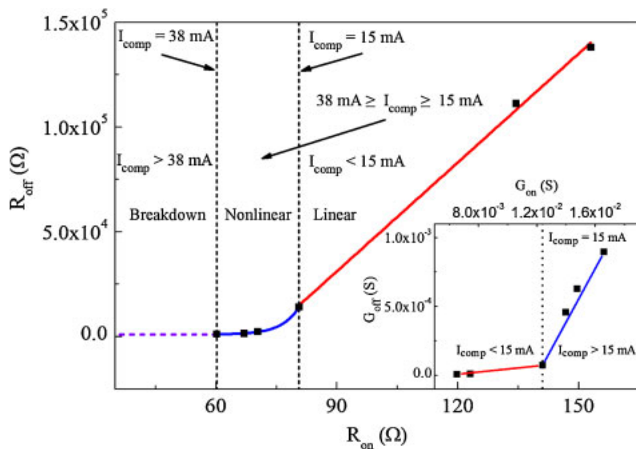

Fig. 7. (Color online) Relationship between R_{off} and R_{on} shows three successive regions as I_{comp} increases: linear region ($I_{comp} < 15$ mA), nonlinear region ($15 \leq I_{comp} \leq 38$ mA), and breakdown region ($I_{comp} > 38$ mA). The solid line, solid curve, and extension dash curve are guide for the eyes. The inset shows G_{off} increases with G_{on}.

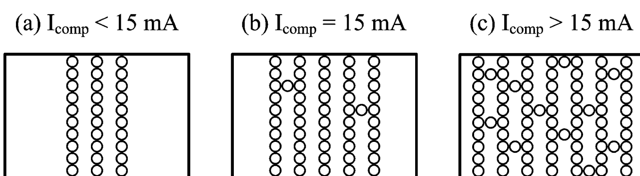

Fig. 8. (a) Few separate CFs ($I_{comp} < 15$ mA). (b) Many CFs begin to connect to each other ($I_{comp} = 15$ mA). (c) Many CFs connect to each other to form a CF network ($I_{comp} > 15$ mA).

CFs is small, the CFs are separated from each other, so the switching properties are only determined by the CFs rather than the remaining part of the thin film, that is the linear region [Fig. 8(a)]; for $I_{comp} = 15$ mA, the number of the oxygen vacancies increases and more CFs form, as a result, some CFs begin to connect with each other, which makes the transport behavior of the film start to show an essential change [Fig. 8(b)]; for $I_{comp} > 15$ mA, high-Joule heating generates large quantities of CFs, which connect to each other to form a complex-connected CF network, and eventually a new different transport behavior is achieved — that is, the nonlinear region [Fig. 8(c)]; for $I_{comp} > 38$ mA, the CF network becomes more conductive and generates more Joule heat at such a high current, and eventually the device breaks down. Compared with the nonlinear region, the linear region is more suitable for memory device applications owing to its low current (low power) and high OFF/ON resistance ratio, and being far from hard breakdown region, which are very important for designing highly sable and reproducible devices. Consequently, it is very important to control and adjust the critical linear–nonlinear transition point of I_{comp} to obtain a proper working range of I_{comp} values. The influence of I_{comp} can also be understood from the inset of Fig. 7. It shows that G_{off} increases nearly linearly with G_{on}, which can be denoted as $G_{off} = kG_{on} + c$, where both k and c are constants. However, k has two different values, $k_1 = 1.15 \times 10^{-2}$ and $k_2 = 1.96 \times 10^{-1}$, for $I_{comp} < 15$ mA and $I_{comp} > 15$ mA, respectively. $k_2/k_1 = 17$ indicates G_{off} depends strongly on G_{on} at high I_{comp} since large quantities of CFs are created, and a rapid increase in G_{off} occurs, which finally leads to the device breakdown. For low I_{comp}, because of a small number of CFs, G_{off} depends weakly on G_{on}. It should be noted that although device breakdown is harmful for bistable memory switching, it may have some useful applications, e.g., it can be used to design read-only memory (ROM).

4. Summary and Conclusions

We successfully fabricated the $Ti/ZrO_2/Pt$ resistive switching devices by a simple sol–gel process. In the ZrO_2-based resistive switching devices, unipolar resistive switching behaviors including bistable memory and monostable threshold switching were measured. The device exhibiting a multilevel resistive switching under different current compliances was studied. As the compliance current increases, the relationship between R_{off} and R_{on} shows three successively regions — the linear, nonlinear, and breakdown regions. To achieve stable switching properties, the resistive switching devices should work in the linear region. Physical mechanisms based on the CF model are responsible for the resistive switching phenomena and the device breakdown. The figure of merit Z of the ZrO_2-based switching device is higher than 10^3. In this study, the memory device with good properties such as unipolar resistive switching, multilevel resistive switching (at least six levels), good scalability, low operation voltage (<5 V), high OFF/ON resistance ratio ($>10^3$), nondestructive readout, long retention ($>10^4$ s), and simple fabrication method is fabricated. Such a ZrO_2-based switching device has promising applications in next-generation nonvolatile memory.

© 2013 The Japan Society of Applied Physics

Acknowledgments

The authors thank Mr. Jun-Sheng Hsu for his help in fabricating Ti top electrodes. This work was supported by the National Science Council (NSC), Taiwan, under project NSC 96-2628-E009-166-MY3. Guo-Yong Zhang would like to express thanks to the postdoctoral fellowship sponsored by NSC of Taiwan. The authors would like to thank the Nano Facility Center at National Chiao Tung University and National Nano Device Laboratories, where some experiments in this study were performed.

1) S. M. Sze and K. K. Ng: *Physics of Semiconductor Devices* (Wiley, New York, 2007) 3rd ed., p. 351.
2) D. Kahng and S. M. Sze: Bell Syst. Tech. J. **46** (1967) 1288.
3) C. Y. Liu, A. Wang, W. Y. Jang, and T. Y. Tseng: J. Phys. D **39** (2006) 1156.
4) C. C. Lin, C. Y. Lin, M. H. Lin, C. H. Lin, and T. Y. Tseng: IEEE Trans. Electron Devices **54** (2007) 3146.
5) M. H. Lin, M. C. Wu, C. H. Lin, and T. Y. Tseng: IEEE Trans. Electron Devices **57** (2010) 1801.
6) C. Y. Lin, C. Y. Liu, C. C. Lin, and T. Y. Tseng: J. Electroceram. **21** (2008) 61.
7) Y. Sato, K. Tsunoda, K. Kinoshita, H. Noshiro, M. Aoki, and Y. Sugiyama: IEEE Trans. Electron Devices **55** (2008) 1185.
8) R. Waser and M. Aono: Nat. Mater. **6** (2007) 833.
9) R. Waser, R. Dittmann, G. Staikov, and K. Szot: Adv. Mater. **21** (2009) 2632.
10) A. Sawa: Mater. Today **11** [6] (2008) 28.
11) S. Seo, M. J. Lee, D. H. Seo, E. J. Jeoung, D. S. Suh, Y. S. Joung, I. K. Yoo, I. R. Hwang, S. H. Kim, I. S. Byun, J. S. Kim, J. S. Choi, and B. H. Park: Appl. Phys. Lett. **85** (2004) 5655.
12) D. Ielmini, C. Cagli, and F. Nardi: Appl. Phys. Lett. **94** (2009) 063511.
13) C. Y. Lin, C. Y. Wu, C. Y. Wu, T. Y. Tseng, and C. M. Hu: J. Appl. Phys. **102** (2007) 094101.
14) C. Schindler, S. C. P. Thermadam, R. Waser, and M. N. Kozicki: IEEE Trans. Electron Devices **54** (2007) 2762.
15) S. Y. Wang, D. Y. Lee, T. Y. Tseng, and C. Y. Lin: Appl. Phys. Lett. **95** (2009) 112904.
16) M. J. Lee, Y. Park, B. S. Kang, S. E. Ahn, C. Lee, K. Kim, W. X. Xianyu, G. Stefanovich, J. H. Lee, S. J. Chung, Y. H. Kim, C. S. Lee, J. B. Park, I. G. Baek, and I. K. Yoo: IEDM Tech. Dig., 2007, p. 771.
17) M. J. Lee, S. I. Kim, C. B. Lee, H. X. Yin, S. E. Ahn, B. S. Kang, K. H. Kim, J. C. Park, C. J. Kim, I. Song, S. W. Kim, G. Stefanovich, J. H. Lee, S. J. Chung, Y. H. Kim, and Y. Park: Adv. Funct. Mater. **19** (2009) 1587.
18) T. Lee and Y. Chen: MRS Bull. **37** [2] (2012) 144.
19) D. S. Shang, L. D. Chen, Q. Wang, W. Q. Zhang, Z. H. Wu, and X. M. Li: Appl. Phys. Lett. **89** (2006) 172102.
20) A. Sawa, T. Fujii, M. Kawasaki, and Y. Tokura: Appl. Phys. Lett. **88** (2006) 232112.
21) M. Fujimoto, H. Koyama, S. Kobayashi, Y. Tamai, N. Awaya, Y. Nishi, and T. Suzuki: Appl. Phys. Lett. **89** (2006) 243504.
22) C. Y. Lin, C. Y. Wu, C. Y. Wu, T. C. Lee, F. L. Yang, C. Hu, and T. Y. Tseng: IEEE Electron Device Lett. **28** (2007) 366.
23) C. Y. Lin, C. Y. Wu, C. Y. Wu, C. C. Lin, and T. Y. Tseng: Thin Solid Films **516** (2007) 444.
24) C. Y. Lin, S. Y. Wang, D. Y. Lee, and T. Y. Tseng: J. Electrochem. Soc. **155** (2008) H615.
25) S. Y. Wang, D. Y. Lee, T. Y. Huang, J. W. Wu, and T. Y. Tseng: Nanotechnology **21** (2010) 495201.
26) D. Y. Lee, S. Y. Wang, and T. Y. Tseng: J. Electrochem. Soc. **157** (2010) G166.
27) S. Y. Wang, C. H. Tsai, D. Y. Lee, C. Y. Lin, C. C. Lin, and T. Y. Tseng: Microelectron. Eng. **88** (2011) 1628.
28) M. C. Wu, Y. W. Lin, W. Y. Jang, C. H. Lin, and T. Y. Tseng: IEEE Electron Device Lett. **32** (2011) 1026.
29) D. Y. Lee and T. Y. Tseng: IEEE Electron Device Lett. **33** (2012) 803.
30) D. Y. Lee, I. C. Yao, and T. Y. Tseng: Jpn. J. Appl. Phys. **51** (2012) 02BJ04.
31) M. C. Wu, W. Y. Jang, C. H. Lin, and T. Y. Tseng: Semicond. Sci. Technol. **27** (2012) 065010.
32) M. C. Wu, T. H. Wu, and T. Y. Tseng: J. Appl. Phys. **111** (2012) 014505.
33) C. Y. Lin, D. Y. Lee, S. Y. Wang, C. C. Lin, and T. Y. Tseng: Surf. Coatings Technol. **203** (2008) 480.
34) S. Y. Wang, C. W. Huang, D. Y. Lee, T. Y. Tseng, and T. C. Chang: J. Appl. Phys. **108** (2010) 114110.
35) D. Y. Lee and T. Y. Tseng: J. Appl. Phys. **110** (2011) 114117.
36) S. Kim, J. Choi, B. H. Park, C. W. Lee, J. Chung, and S. Seo: J. Korean Phys. Soc. **53** (2008) 700.
37) D. K. Yun, K. D. Kim, S. Kim, J. H. Lee, H. H. Park, J. H. Jeong, Y. K. Choi, and D. G. Choi: Nanotechnology **20** (2009) 445305.
38) H. K. Yoo, S. B. Lee, J. S. Lee, S. H. Chang, M. J. Yoon, Y. S. Kim, B. S. Kang, M. J. Lee, C. J. Kim, B. Kahng, and T. W. Noh: Appl. Phys. Lett. **98** (2011) 183507.
39) C. Y. Lin, D. Y. Lee, S. Y. Wang, C. C. Lin, and T. Y. Tseng: Surf. Coatings Technol. **203** (2008) 628.
40) Y. T. Tsai, T. C. Chang, C. C. Lin, S. C. Chen, C. W. Chen, S. M. Sze, F. S. Yeh, and T. Y. Tseng: Electrochem. Solid-State Lett. **14** (2011) H135.
41) S. Kim and Y. K. Choi: Appl. Phys. Lett. **92** (2008) 223508.
42) Y. T. Tsai, T. C. Chang, C. C. Lin, L. S. Chiang, S. C. Chen, S. M. Sze, and T. Y. Tseng: ECS Trans. **41** [3] (2011) 475.
43) M. Haemori, T. Nagata, and T. Chikyow: Appl. Phys. Express **2** (2009) 061401.
44) D. Panda, C. Y. Huang, and T. Y. Tseng: Appl. Phys. Lett. **100** (2012) 112901.
45) S. Lee, W. G. Kim, S. W. Rhee, and K. Yong: J. Electrochem. Soc. **155** (2008) H92.
46) S. J. Song, K. M. Kim, G. H. Kim, M. H. Lee, J. Y. Seok, R. Jung, and C. S. Hwang: Appl. Phys. Lett. **96** (2010) 112904.
47) K. Tsunoda, Y. Fukuzumi, J. R. Jameson, Z. Wang, P. B. Griffin, and Y. Nishi: Appl. Phys. Lett. **90** (2007) 113501.
48) I. C. Yao, D. Y. Lee, T. Y. Tseng, and P. Lin: Nanotechnology **23** (2012) 145201.
49) H. Sim, D. Choi, D. Lee, S. Seo, M. J. Lee, I. K. Yoo, and H. Hwang: IEEE Electron Device Lett. **26** (2005) 292.
50) K. Kinoshita, T. Tamura, M. Aoki, Y. Sugiyama, and H. Tanaka: Appl. Phys. Lett. **89** (2006) 103509.
51) M. H. Lin, M. C. Wu, C. Y. Huang, C. H. Lin, and T. Y. Tseng: J. Phys. D **43** (2010) 295404.
52) M. H. Lin, M. C. Wu, C. H. Lin, and T. Y. Tseng: J. Appl. Phys. **107** (2010) 124117.
53) M. H. Lin, M. C. Wu, Y. H. Huang, C. H. Lin, and T. Y. Tseng: IEEE Trans. Electron Devices **58** (2011) 1182.
54) Y. T. Tsai, T. C. Chang, W. L. Huang, C. W. Huang, Y. E. Syu, S. C. Chen, S. M. Sze, M. J. Tsai, and T. Y. Tseng: Appl. Phys. Lett. **99** (2011) 092106.
55) H. Choi, M. Pyun, T. W. Kim, M. Hasan, R. Dong, J. Lee, J. B. Park, J. Yoon, D. J. Seong, T. Lee, and H. Hwang: IEEE Electron Device Lett. **30** (2009) 302.
56) K. Oka, T. Yanagida, K. Nagashima, H. Tanaka, and T. Kawai: J. Am. Chem. Soc. **131** (2009) 3434.
57) T. Kever, U. Bottger, C. Schindler, and R. Waser: Appl. Phys. Lett. **91** (2007) 083506.
58) C. Y. Liu and T. Y. Tseng: J. Phys. D **40** (2007) 2157.
59) M. H. Lin, M. C. Wu, C. C. Lin, and T. Y. Tseng: Ferroelectrics **380** (2009) 30.
60) C. B. Lee, B. S. Kang, A. Benayad, M. J. Lee, S. E. Ahn, K. H. Kim, G. Stefanovich, Y. Park, and I. K. Yoo: Appl. Phys. Lett. **93** (2008) 042115.

© 2013 The Japan Society of Applied Physics